Applied Catalysis B: Environmental 237 (2018) 911–918

Contents lists available at ScienceDirect

Applied Catalysis B: Environmental

journal homepage: www.elsevier.com/locate/apcatb

Reducing the onset potential of CO_2 electroreduction on CuRu bimetallic particles

Joshua T. Billy, Anne C. Co*

Department of Chemistry and Biochemistry, The Ohio State University, 100 W 18th Avenue, Columbus, Ohio 43210, USA

ARTICLE INFO

Keywords:
CO_2electroreduction
Electrocatalysis
Copper nanoparticles
Bimetallic catalyst
Ruthenium

ABSTRACT

Lower onset potentials for hydrocarbon products were observed during the electrochemical reduction of carbon dioxide (CO_2RR) on copper particles (40–60 nm) coated with a thin layer of ruthenium via galvanic displacement, referred to as Ru@Cu. Hydrocarbons detected include ethane, ethylene, acetate, ethanol, propanol and CO. In the case of ethane (C_2H_6), the onset potential is 200 mV lower on Ru@Cu than on bare Cu particles. Increasing Ru coverage decreases the CO_2RR activity while hydrogen evolution (HER) activity increased substantially. An optimum Ru coverage was found when the displacement was performed for 10 s. The results presented here highlight the importance of surface chemistry in determining reaction selectivity.

1. Introduction

A net-zero carbon emission fuel cycle can be realized by pairing renewable energy generation with carbon dioxide reduction reaction (CO_2RR) to form useful hydrocarbons. A variety of electrocatalysts have been studied for CO_2RR, but among pure metals only copper can catalytically convert carbon dioxide to multicarbon products in significant quantities at room temperature and atmospheric pressure [1,2]. It is hypothesized that CO_2 electroreduction largely depends on the adsorption energy of the various intermediate species in dictating the overall selectivity of electrolysis [3–8], partially explaining why copper can catalyze reactions requiring > $2e^-$ and metals such as gold primarily produce CO, while platinum is unreactive towards CO_2 in aqueous solutions [2]. Copper's moderate adsorption energy for intermediate species such as CO, depicted in a Sabatier plot [6,4–8], is often cited for its favorable performance in CO_2RR [9,10]. However, other properties have equal importance in aspects of the reaction. For example, highly nanostructured materials are often used in catalysis to increase reaction activity, and in the case of CO_2RR, nanostructured copper also provides unique selectivity [11,12]. It has been reported that the local pH [1,13] and grain boundaries [14,15] are largely responsible for the enhanced electrochemical properties of nanostructured catalysts. And recently, the presence of subsurface oxygen in oxide-derived copper catalysts has been observed and may be essential for the stabilization of adsorbed intermediates in the electroreduction of CO_2 to multicarbon species due to alterations in the catalyst's electronic structure [16,17].

Experiments on nanostructured copper catalysts typically favor production of multicarbon hydrocarbon species rather than single carbon species such as methane or CO [18,19]. Increasing the CO binding energy is expected to further enhance C—C coupling. However, once the CO binding energy becomes too great, such as when using Pt, Ni, and Ru metal catalysts, CO will poison the catalyst surface and lead to decreased CO_2RR activity.

In this work, Ru was chosen due to its strong CO adsorption and effectiveness in a variety of catalytic reactions [20]. Ru is a highly active catalyst in the gas phase conversion of CO_2 to CH_4. In CO_2RR research, Ru catalysts have been used with varying degrees of success. Ruthenium-based molecular catalysts have been studied for the electrochemical conversion of CO_2 to CO and formate [21,22]. In heterogeneous electroreduction of CO_2, ruthenium metal and its oxide are selective for CH_4 and CH_3OH [23,24], and recent work with Ru/C coated gas diffusion electrodes observed small amounts of methanol as well as other alcohols, such as ethanol and isopropanol [25]. Based on these studies, we hypothesized that thin layers of ruthenium deposited on copper nanoparticles could modify the CO_2RR product selectivity to favor more reduced species.

Herein, we report a study on ruthenium coated copper nanoparticles catalyzing the electroreduction of CO_2. Ruthenium deposition was performed via galvanic displacement, where longer displacement times resulted in thicker layers of ruthenium. We show that an optimal Ru coverage reduces the onset potential of a majority of CO_2 products detected while thick Ru coverage results in HER outcompeting CO_2RR. This work illustrates how bimetallic materials can alter the CO_2RR product selectivity in a desirable fashion.

* Corresponding author.
E-mail address: co@chemistry.ohio-state.edu (A.C. Co).

https://doi.org/10.1016/j.apcatb.2018.06.072
Received 27 November 2017; Received in revised form 26 June 2018; Accepted 27 June 2018
Available online 28 June 2018
0926-3373/

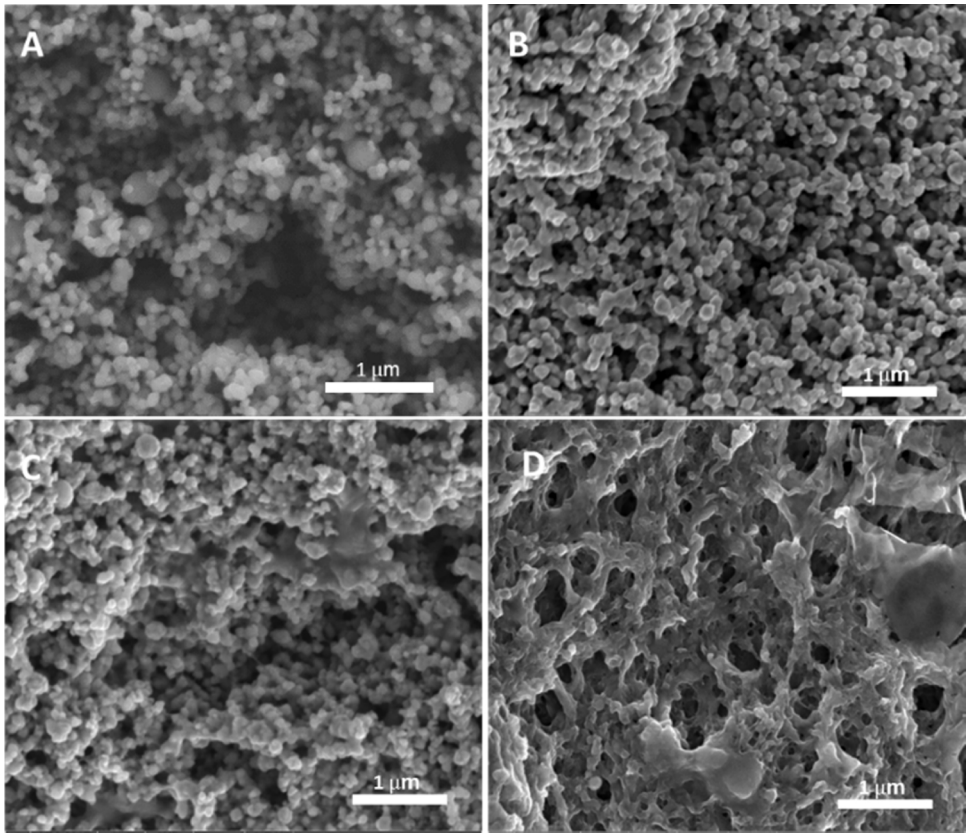

Fig. 1. SEM images of a (A) copper nanoparticle electrode and copper nanoparticle electrodes displaced with ruthenium for (B) 10 s, (C) 2 min, and (D) 1 h. Images were collected on a FEI Helios Nanolab 600 SEM for Fig. 1A and a FEI Sirion SEM for Fig. 1B–D.

2. Experimental

2.1. Electropolishing Cu foils

Copper foil (Sigma Aldrich, 99.99%) was cut to the appropriate size (8 cm × 4.5 cm × 0.5 mm) and electropolished in 85% phosphoric acid (Fisher Scientific, certified ACS) at an oxidation potential of around 1.8 V vs. Ag/AgCl for 5 min. The polishing potential was chosen to be after the Cu oxidation peak and before water oxidation. The actual oxidation potential was determined for each foil by performing an initial linear voltammetry sweep in the 85% phosphoric acid solution. The foil was then rinsed and sonicated (FS30D, Fisher Scientific) in deionized water (DI, MilliQ, Advantage A10), for 5 min before casting the Cu particles.

2.2. Preparation of CuRu particles

Cu particles were purchased from SkySpring Nanomaterials, Inc. According to the manufacturer, these Cu nanoparticles were made via electrical explosion method and were 40–60 nm in diameter, on average. The particle size was confirmed in this work by SEM imaging (Fig. 1).

To create a suspension, 50 mg of Cu particles were mixed with 3 mL of methanol and sonicated for 10 min. 50 u L of a 5% w/w Nafion in water and 1-propanol solution (Alfa Aesar) was added to the suspension and the solution was sonicated for an additional 10 min. Immediately after sonication, the mixture was poured overtop the electropolished Cu foil enclosed in a rectangular holder and placed in a furnace at 70 °C for 1 h or until dried. Approximately 0.100 g of $RuCl_3$ x H_2O (Pressure Chemical Co.) was weighed out and dissolved in 300 mL of DI water. The mixture was heated to 50 °C and purged with N_2 gas for 30 min while stirring. The Cu particle coated foil was submerged into the Ru solution for a specified length of time (between 10 s and 60 min) while stirring to allow galvanic displacement of Cu for Ru. Upon removal from the Ru solution, the electrodes were rinsed in DI water, dried with N_2, and sealed in air free bags until use.

The electrodes not displaced with Ru will be referred to as Cu NP and the electrodes displaced with Ru will be referred to as Ru@Cu NP.

2.3. Electrolyte solution preparation

A 2 M stock solution of potassium bicarbonate (Fisher Scientific, USP/FCC grade) electrolyte was prepared with deionized water with a total organic count of < 2 ppb (MilliQ, Advantage A10). The stock solution was pre-electrolyzed at 2.0 V, at roughly 5 mA/cm^2, for 24 h using dimensionally stabilized anode (DSA®, de Nora) as electrodes. The solution was then filtered before use. Diluted concentrations of $KHCO_3$ were prepared from the 2 M pre-electrolyzed stock solution.

2.4. Electrochemical cell

Experiments were performed at ambient temperature and pressure in a custom acrylic two-compartment electrochemical cell. A schematic of this cell can be found in Ref. [26]. The two compartments were separated by a Selemion AMV anion exchange membrane (AGC Engineering Co.) and sealed using Viton® gaskets. The counter electrode was a DSA® (de Nora) plate placed parallel to the working electrode, which was 1.2 cm away from the anion exchange membrane separator, resulting in a 27.9 mL total volume in the working electrode compartment. The volume of solution in the counter electrode compartment was 26 mL. The geometric surface area of both electrodes was 26 cm^2. The electrolyte used was 0.1 M $KHCO_3$ saturated with CO_2 (pH 6.8). The electrolyte was continuously flowed into the cell at a controlled rate of 1.7 mL/min. After exiting the cell, the electrolyte was either

collected for analysis or disposed of. Electrolyte containing products was not recycled back into the electrochemical cell to ensure that the working electrode surface was always exposed to freshly saturated CO_2 solution. In addition to flowing a saturated solution of CO_2 into the WE compartment, a gas dispersion tube (Ace Glass, d = 7 mm, center 5 mm away from WE) was inserted into the working electrode compartment providing a controlled CO_2 gas flow rate of ca. 20 mL/min.

Headspace gas was vented directly to the gas chromatograph (7890 A, Agilent Technologies) and injected into the column through a sampling loop that sampled continuously every 13 min. The combined CO_2 and product gas flow rate was measured at the end of the sampling loop by a soap bubble flow meter (Model 520, Fisher Scientific). A hydrogen reference electrode was created by flowing H_2 over a piece of platinized Pt gauze in the 0.1 M $KHCO_3$ electrolyte (pH 9.2) in a separate compartment with a Luggin capillary. All of the potentials reported are referenced against a reversible hydrogen electrode (RHE) at the same pH as the solution containing the reactant.

2.5. Electrolysis experiments

Potentiostatic experiments were performed using a Model 253 A, Princeton Applied Research pontentiostat and a Biologic VSP potentiostat. For each experiment, a linear potential sweep was obtained starting at the open circuit potential (OCP) to the potential of interest at 50 mV/s, where it was held for 1 h, unless stated otherwise.

Data was collected against a hydrogen electrode in 0.1 M $KHCO_3$ solution (pH 9.2). We have verified that the potential of the hydrogen electrode is stable as long as H_2 is continuously supplied. Data reported herein is presented against a RHE at pH 6.8, which is the pH of a CO_2 saturated 0.1 M $KHCO_3$. The actual pH of both the unsaturated and saturated bicarbonate solution was measured before the experiment. The potential reported here was corrected using the following equation: $E_{corrected}$ (vs. RHE) = $E_{measured}$ − 0.059*($9.2_{pH\ of\ RHE}$ − $6.8_{pH\ of\ solution}$).

2.6. Product analysis

Headspace gas from the electrochemical reactor was introduced into the gas chromatograph through a series of two gas sampling loops. Automatic injections occurred every 13 min. The first gas sampling-loop is connected to a quadrupole mass spectrometer through a CP-PoraBond Q capillary column and the second loop is connected to a thermal conductivity detector through Haysep Q and Molseive 5 A columns. The mass spectrometer was used to quantify hydrocarbons (CH_4, C_2H_4, and C_2H_6). The thermal conductivity detector was used to quantify H_2 and CO concentrations.

The liquid in the working compartment of the electrolysis cell was collected at various intervals during the experiment and analyzed using an AVIII 400 MHz NMR spectrometer. NMR samples were prepared by mixing 0.8 mL of the collected solution with 0.1 mL D_2O and 0.1 mL of 100 ppm acetonitrile as an internal standard. A water suppression method was used to measure the ^1H spectrum. This allowed for identification and quantification of formate, acetate, methanol, ethanol, and propanol, as well as trace amounts of other carbonaceous species.

2.7. Calculating Faradaic efficiency and CO_2 consumption rate

Faradaic efficiency was calculated using Eq. (1) where eff is the Faradaic efficiency, Q_p is the charge required to form the measured amount of product p, and Q_T is the total charge passed. CO_2 consumption rates (mol/cm^{2}s) were calculated from Eq. (2) where j is the total current density, F is the Faradaic constant, n is the number of CO_2 molecules required for the reaction, and z is the number of electrons required to form product p.

$$eff(\%) = \frac{Q_p}{Q_T} * 100 \quad (1)$$

$$CO_{2\ consumption\ rate} = \left(\frac{j}{F}\right)\sum_p \left(\frac{n * eff}{z}\right)_p \quad (2)$$

2.8. Catalyst characterization

2.8.1. Scanning electron microscopy (SEM)

The nanostructure of the catalysts was characterized using scanning electron microscopy (SEM). Imaging of the particles was performed using the secondary electron detector on a FEI Sirion SEM and a FEI Helios Nanolab 600 SEM before and after drop casting them onto a copper electrode and after electrolysis. The working distance was approximately 5 mm and the accelerating voltage was set to 10 kV.

2.8.2. X-ray photoelectron spectroscopy (XPS)

X-ray photoelectron spectroscopy (XPS) was used to analyze the surface chemical state of the Cu and Ru@Cu catalysts. XPS spectra were obtained on a Kratos Axis Ultra spectrometer using monochromatic Al Kα radiation (hυ = 1486.6 eV). The analysis area was 300 × 700 μm^2. Core peaks were recorded with a step energy of 0.1 eV and a pass energy of 20 eV. All binding energies were calibrated from the adventitious carbon contamination peak using the C 1 s peak at 285.0 eV. CasaXPS software was used for peak fitting. Peaks were fitted using the minimum number of components required to provide a good fit. Peaks were fit using a nonlinear Shirley-type background and a 70% Gaussian, 30% Lorentzian peak shape. In the case a Shirley-type background did not provide a good fit, a linear background was used. Quantification was performed based on atomic sensitivity factors.

2.8.3. X-ray powder diffraction (XRD)

Powder diffraction patterns were collected using a Cu Kα source (1.54 Å) on a Rigaku XRD. The scans were collected from 10 to 100 degrees (2 theta) at a scan rate of 5 degrees per minute.

3. Results and discussion

The Cu particles were uniform in size and shape. According to the manufacturer, the nanoparticles were expected to be 40–60 nm on average, and this size distribution can be estimated from the SEM images shown in Fig. 1. As-received nanoparticles were spherical in shape, mostly monodispersed, but small cluster agglomerates and occasionally porous clusters comprised of several hundred particles were also observed. After drop casting, the Cu particles remained spherical and had high coverage on the electrode surface, as shown in Fig. 1A. The Cu particle electrode appeared to be highly porous. The addition of ruthenium via galvanic displacement had varying effects on the nanoparticle shape and overall porosity as a function of displacement time. A 10 s displacement had no noticeable effect, shown in Fig. 1B. As the displacement time increased to two minutes, the porosity of the nanoparticle covered surface appeared to decrease, as the pores were filed in with ruthenium. Due to the galvanic displacement reaction occurring at elevated temperature, it is possible that some copper dissolved and redeposited on the surface, which could further alter the structure. Drastic changes were observed when the displacement time was increased to 1 h. The material no longer resembled a nanoparticle covered surface and instead appeared web-like, as seen in Fig. 1D. Few individual nanoparticles can be discerned and it appeared that nanoparticle clusters aggregated together. These SEM images agree with XPS results to confirm that extended galvanic displacement times increase ruthenium coverage.

The X-ray diffraction (XRD) patterns of the Cu particles showed characteristic Cu (111), (200), and (220) peaks (Fig. 2). Using the Scherer equation, the crystallite sizes for the SkySpring Cu were calculated to be a minimum of 40 nm. The Scherer equation uses peak broadening to estimate the nanoparticle size, but inhomogeneous strain and other factors contribute to broadening. The calculation for the

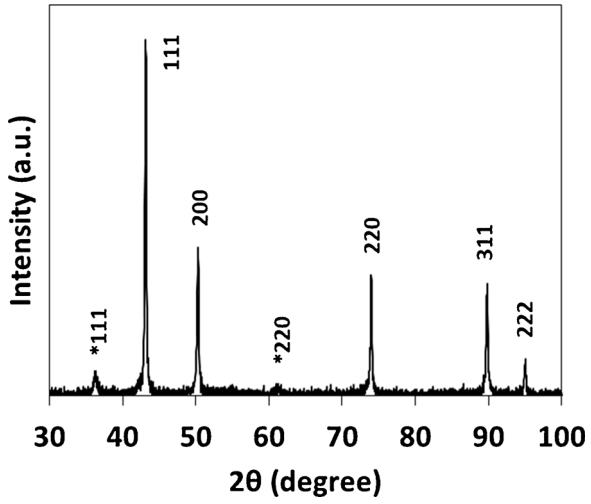

Fig. 2. X-ray diffraction pattern of copper nanoparticles. Cu_2O peaks indicated by (*).

SkySpring particle size agrees with SEM estimates. Small peaks confirming Cu_2O were observed on the SkySpring particles, agreeing with XPS results. Oxides were likely formed due to handling of the particles in air.

Table 1
Copper/ruthenium atomic % ratios as a function of galvanic displacement time in $RuCl_3$ x H_2O obtained via high resolution XPS analysis of the Cu 2p and Ru 3p peak.

Cu/Ru	10 s	2 min	10 min	1 h
Surface	1.1	1.1	0.2	0.25
45 s etch	8.9	6.5	N/A	N/A
90 s etch	13.0	9	N/A	N/A

X-ray photoelectron spectroscopy was used to quantify copper and ruthenium at the electrode surface and provide chemical state information. Survey scans on all electrodes confirm only the presence of copper, ruthenium, oxygen, carbon, and fluorine (from the Nafion polymer), shown in Fig. 3A. As all samples were handled in air before XPS was performed, surface oxide was observed and could only be partially removed by argon ion etching due to the porous nature of the samples. High resolution XPS scans show that as-prepared copper particle electrodes contain significant CuO (234.0 eV, Fig. 3B). The catalyst surface after electrolysis gave Cu_2O (232.3 eV) and Cu° (232 eV) signatures (Fig. 3C) [27]. The decrease in Cu $2p_{3/2}$ peaks at higher binding energy and the reduction of Cu^{2+} satellite peaks in XPS scans post-electrolysis were used to infer the change in Cu oxidation state. Since

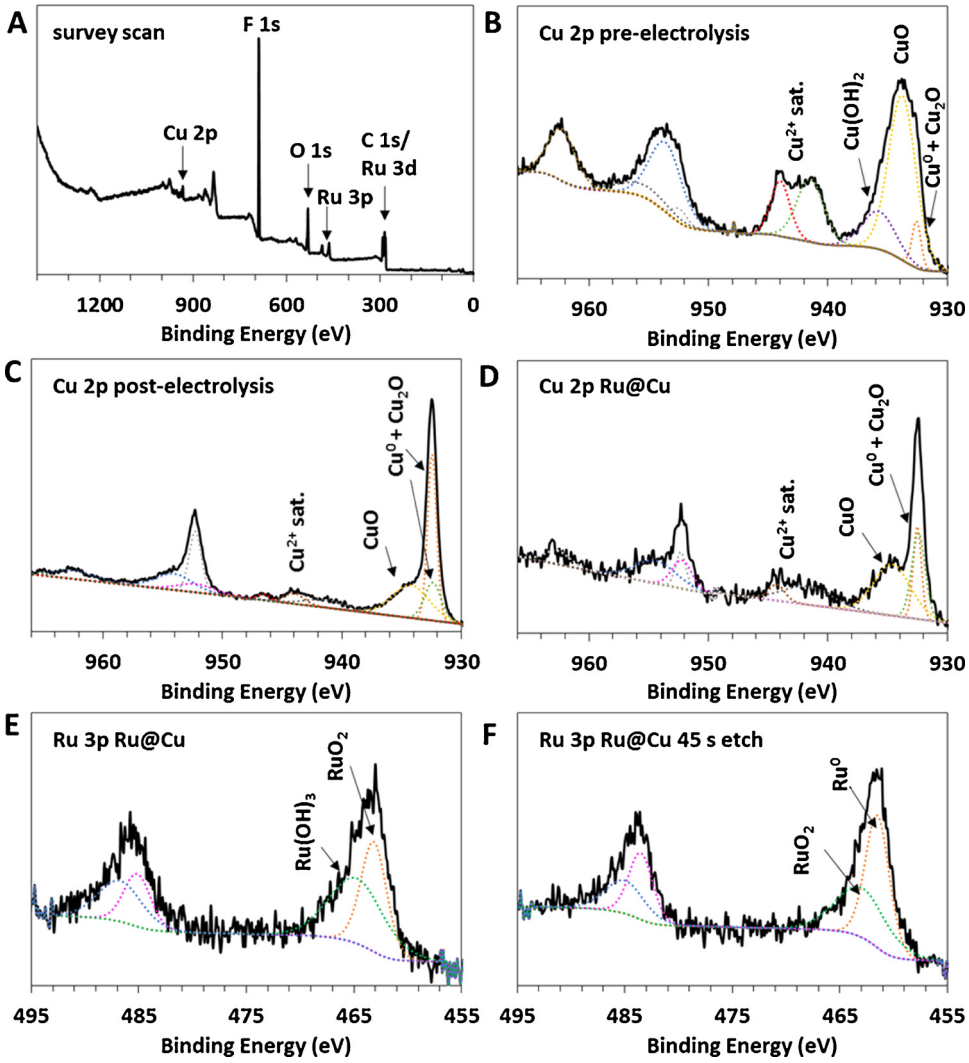

Fig. 3. X-ray photoelectron spectroscopy was used to examine the chemical state of bare copper particle electrodes (Fig. 1A–C) and Ru@Cu electrodes prepared with a 10 s Ru displacement time (Fig. 1D–F). High resolution XPS of the Cu 2p and Ru 3p regions was used for chemical state analysis and elemental quantification.

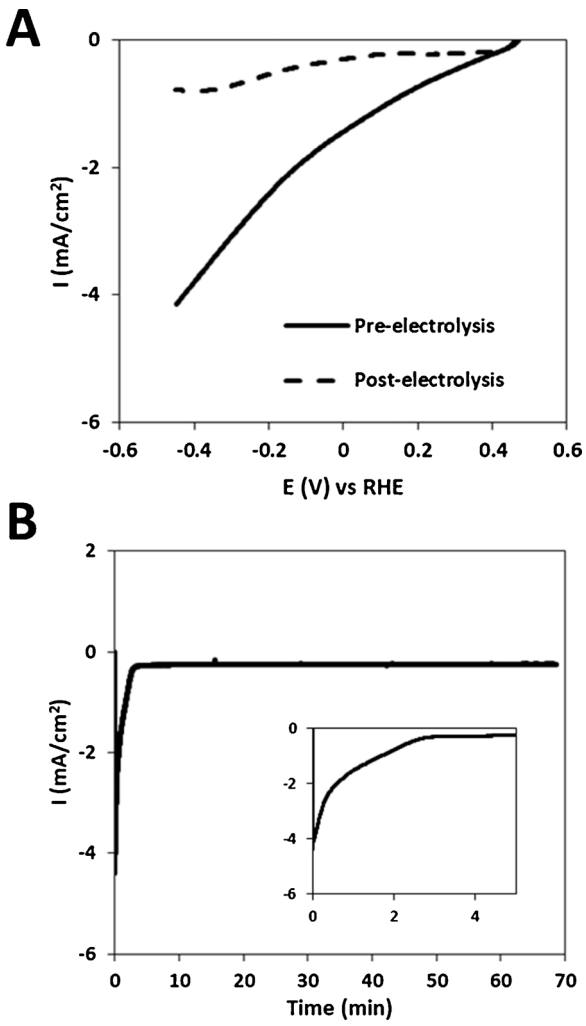

Fig. 4. (A) Linear sweep voltammograms on copper nanoparticle electrode from OCP to −0.45 V vs RHE pre-electrolysis and post-CO_2RR electrolysis; (B) Chronoamperometry (electrolysis) on the same electrode at −0.45 V vs RHE for 65 min in 0.1 M $KHCO_3$ saturated with CO_2.

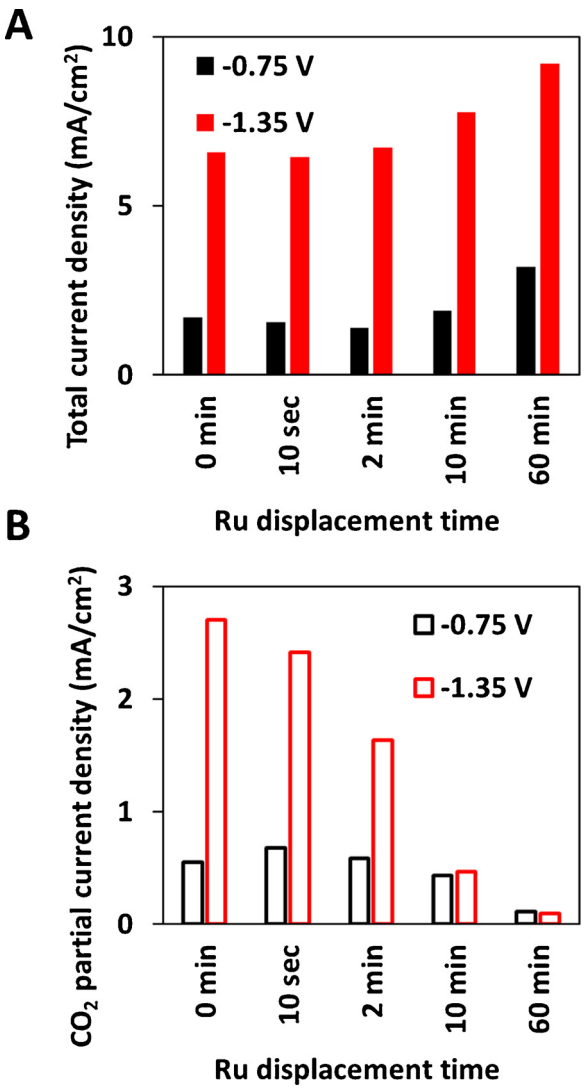

Fig. 5. (A) Total current density and (B) CO_2 partial current density as a function of ruthenium displacement time at −0.75 V and −1.35 V vs RHE.

Ru 3d is in the same region as C 1 s (276–300 eV), all high resolution Ru XPS were reported for the Ru 3p (450–500 eV) region to avoid peak overlap with the C 1 s and allow for more accurate elemental quantification. Ruthenium coated electrodes did not contain a significant amount of CuO (Fig. 3D), and we attribute this to Ru coverage preventing oxidation of Cu. Ruthenium on the surface exists in an oxidized state as RuO_2 (263.1 eV) and a more oxidized form, possibly $Ru(OH)_3$ (264.7 eV, Fig. 3E) [28]. Etching the surface layer revealed metallic Ru° (261.5 eV) and RuO_2 (Fig. 3F). A 10 s displacement was long enough to deposit a significant amount of Ru, resulting in a 1.1/1 Cu/Ru surface atomic % ratio (Table 1). The concentration of Ru present is roughly correlated to the galvanic displacement time, where a longer displacement time results in higher Ru concentration. However, the results in Table 1 show little difference in the Cu/Ru ratio at the surface of the sample between the 10 s and 2 min samples, and the 10 min and 1 h samples, which we attribute to inhomogeneity in XPS spot analysis due to the rough surface and porous nature of the nanoparticle electrodes. When the surface layer was etched away on Ru@Cu electrodes with 10 s and 2 min Ru displacement times, the Ru content decreased slightly and the Cu signal became more pronounced, resulting in an increased Cu:Ru ratio. Etching experiments seem to suggest that longer displacement time allows Ru to reach deeper in to the porous structure, as evidenced by a larger Cu:Ru ratio of 13 for the 10 s deposited Ru at 90 s etch compared to a smaller Cu:Ru ratio of 9 for the 2 min deposition at 90 s etch. The drop in Ru content with depth was most significant for samples prepared with 10 s displacement times. Etching experiments were not performed on 10 min and 1 h Ru@Cu electrodes.

3.1. Electrolysis measurement

Linear sweep voltammetry, LSV, (Fig. 4A) also suggests an oxide layer on the surface of as-prepared Cu particle catalysts. In LSV scans prior to bulk electrolysis, a cathodic current density of nearly 2 mA/cm^2 was measured at potentials positive of HER and CO_2RR. Post-electrolysis, a repeat of the same LSV scan in a 0.1 M $KHCO_3$ saturated with CO_2 revealed a drastic reduction in current density and the presence of small peaks (ca. -0.35 V) typically attributed to adsorption of intermediates. We assign the small peak beginning at -0.35 V in the post-electrolysis scan to CO adsorption on the electrode surface, which prevents H_2 adsorption and thus decreases HER activity [3]. No such peak is observed in the pre-electrolysis scans, possibly indicating that no CO_2RR occurred until after oxide removal. Chronoamperometric measurements suggest that oxide removal continued until a steady state current was obtained as CO_2RR and HER commenced (Fig. 4B). The presence and removal of this oxide layer was verified via XPS (Fig. 3B and C).

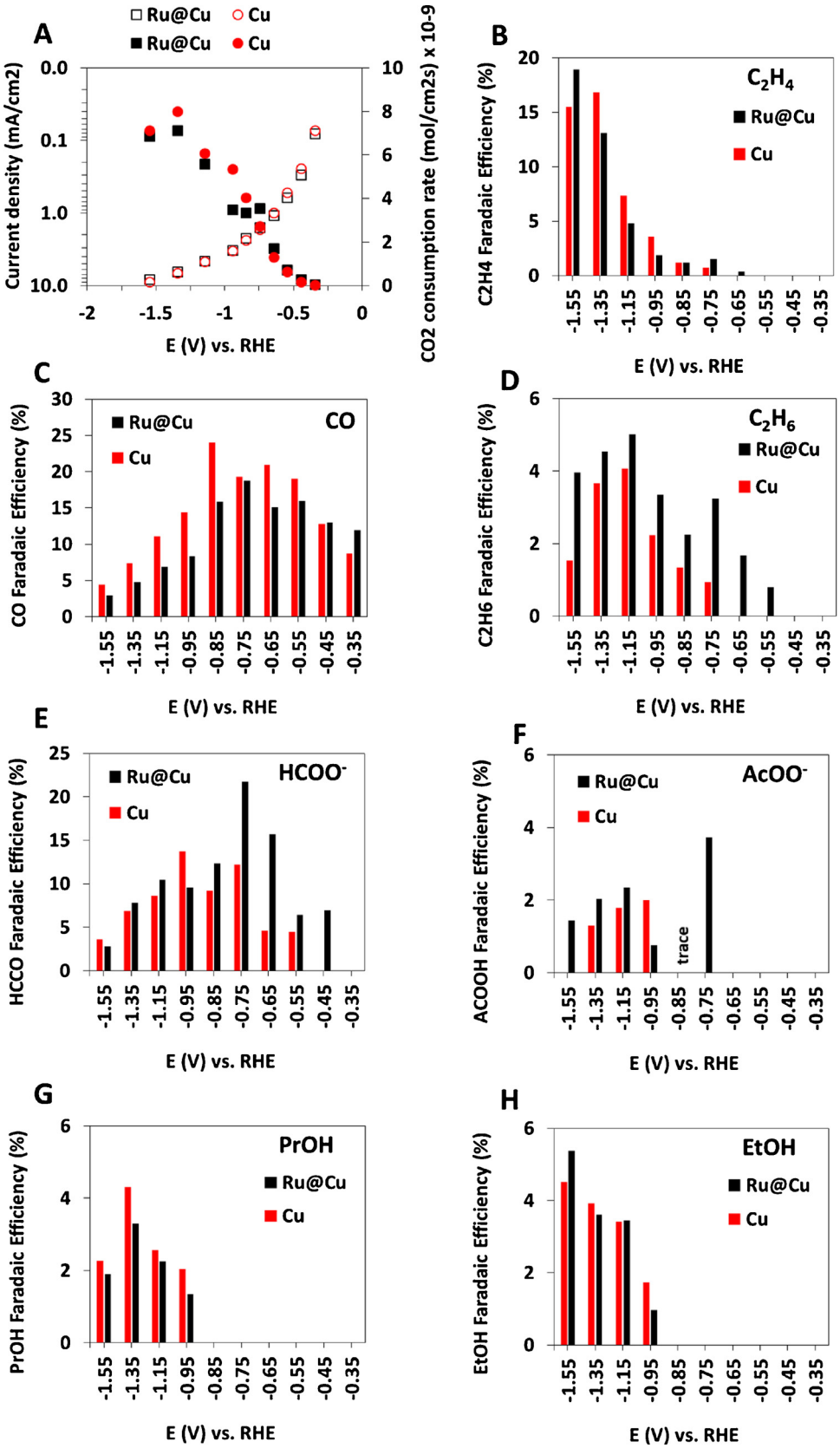

Fig. 6. (A) Total current density (open symbols) and CO_2 consumption rate (filled symbols) as a function of applied potential for Cu and Ru@Cu electrodes. Faradaic efficiency as a function of applied potential for (B) C_2H_4, (C) CO, (D) C_2H_6, (E) HCOOH, (F) acetate (AcOO-), (G) propanol (PrOH), and (H) ethanol (EtOH).

3.2. Catalytic activity of Ru@Cu vs. Cu nanoparticles

The steady state current densities of Ru@Cu (for Ru deposited between 10 s to 60 min), 1 h into the electrolysis at -0.75 and -1.35 V are plotted in Fig. 5. At the potentials tested, the CO_2 reduction reaction and the hydrogen evolution reaction (HER) occur simultaneously, and the total current density is therefore a summation of the current resulting from both reactions. At both -0.75 V and -1.35 V, the total current density measured on Ru@Cu (10 s to 2 min) did not vary much from bare Cu particles. This suggests that minimal Ru deposition did not significantly alter the catalyst nanostructure, where the total surface area was roughly the same, as was confirmed by SEM. As the amount of Ru increased, however, the overall current density increased greatly (Fig. 5A), which can mainly be attributed to the hydrogen evolution reaction, which outcompetes CO_2RR on Ru surfaces (Fig. 5B). The current density remained stable throughout 1 h experiments, with some fluctuations due to bubble formation (Fig. 3B). The total current density did not exceed 10 mA/cm^2 on all catalysts at the overpotentials measured. This is consistent with copper particle catalysts from the literature [29,30], whereas smaller particle sizes (d < 5 nm) are capable of achieving much higher current densities [31]. Alternatively, the overall CO_2RR activity can be significantly increased by increasing mass transport of CO_2 to the electrode surface via use of gas diffusion electrodes [13,26,32].

In Fig. 5B, partial CO_2 current density was obtained by calculating the current that must be consumed to produce all of the detected carbon containing products. The difference between the total current density and the CO_2 partial density is essentially the current that went to produce H_2. The partial CO_2 current is also a measure of the CO_2 consumption rate, which increased as the overpotential became greater. A maximum consumption rate was achieved at -1.35 V vs RHE on both Cu NP and Ru@Cu NP. As we have reported previously [26], under a fixed set of conditions the CO_2 consumption rate reaches a maximum value at high overpotentials (ca. -1.35 V) and begins to decrease as HER takes off. It has been suggested that this is due to increased affinity of H^+ to the polarized electrode when the overpotential is increased to a more negative value, as compared to the neutral and nonpolar CO_2 molecule [33]. In Fig. 5B, we show that at low overpotentials, the deposition of Ru on Cu for 10 s to 2 min resulted in an increase in the overall consumption of CO_2, while the total current density remained very similar. This suggests that the presence of Ru slightly increased the surface's preference for CO_2 adsorption at low overpotentials. However, a further increase in the Ru content (e.g. 10 min and 60 min deposition) reduced the CO_2 consumption rate. The trend of CO_2RR activity versus Ru deposition time measured at -1.35 V suggests that the CO_2RR activity is preferred on a pure Cu surface, possibly due to competing HER reactions at these potentials. Our data suggests that there is a very delicate balance at the catalysts/electrolyte interface that alters the selectivity between HER and CO_2RR even with the smallest changes in the reaction conditions.

3.3. Product selectivity

A total of 10 reaction products were detected in the electrolysis experiments between -0.45 V and -1.55 V vs RHE: H_2, CO, C_2H_4, C_2H_6, $HCOO^-$, CH_3COO^-, ethanol (EtOH), propanol (PrOH), and sometimes CH_4 and CH_3OH. Faradaic efficiencies for the products were calculated and reported in Fig. 6.

Only the 2e$^-$ reduction products, CO, $HCOO^-$, and H_2 were observed on Cu NP and Ru@Cu NP at potentials positive of -0.55 V or at the lower CO2RR overpotential. While other more reduced species are forming at higher overpotentials, CO, $HCOO^-$ and H_2 are typically present at all applied potentials (Fig. 6). Reaction mechanism calculations and experiments indicate HCOO- is a termination product while CO can be further reduced, and often hypothesized as the first intermediate for the formation of all other CO_2RR species detected [1]. The stabilization of CO on copper allows for further electron transfer reactions to occur.

More reduced species, such as C_2H_4 and C_2H_6 were only observed at potentials negative of -0.55 V on the 10 sRu@Cu NP electrode and -0.65 V on the Cu NP electrode. At even more negative potentials, EtOH, PrOH, and AcO^- were also detected. While CH_4 is commonly reported on nanostructured copper catalysts, no CH_4 was detected for the SS Cu NP and only trace amounts (< 0.1% FE) could be detected on the Ru@Cu NP at a very negative potential of -1.55 V. Generally, CH_4 is produced in significant quantities on electropolished Cu foils and reaches 20% FE at −1.55 V. Trace MeOH was detected at -1.35 V on Cu NP but not at any other potential. It is possible that other trace liquid species are formed in the reaction, but they were not produced in large enough quantities to be detected using our NMR method.

The addition of Ru to the Cu NP catalyst lowered the onset potential for the following species by a least 100 mV: C_2H_4, C_2H_6, $HCOO^-$, and CH_3COO^-. For both Cu NP and Ru@Cu NP, C_2H_6 first appeared at lower overpotentials than C_2H_4. C_2H_6 is unique to nanostructured catalysts and is not typically detected on Cu foil. However, the total efficiency for C_2H_6 did not exceed 5% at any of the potentials tested. Cu NP was more selective for C2 species overall, though Ru@Cu NP was more selective toward C_2H_6, which requires 14 e$^-$, than C_2H_4, which requires 12 e$^-$.

4. Conclusions

The galvanic displacement of of Ru on Cu nanoparticle electrodes resulted in a catalyst material, Ru@Cu, with enhanced CO_2RR properties. The increased CO_2RR activity relative to HER, altered product selectivity, and reduced onset potential for several CO_2RR species can likely be attributed to the improved intermediate binding energies of intermediate species on Ru@Cu electrodes. Cu-based materials remain the most promising catalysts for the electrochemical conversion of CO_2 and bimetallic variations of nanostructured copper, such as the addition of Ru, may be the key to achieving good selectivity and high activity. We anticipate that better control of the material's nanostructure and incorporation of Ru will result in a catalyst with improved functionality.

Acknowledgements

This work is supported by the National Science Foundation (NSF CHE 1455162), and in part by the Ohio State University Materials Research Seed Grant Program, and the Ohio State Department of Chemistry and Biochemistry.

References

[1] Y. Hori, A. Murata, R. Takahashi, Formation of hydrocarbons in the electrochemical reduction of carbon dioxide at a copper electrode in aqueous solution, J. Chem. Soc. Faraday Trans. I 85 (1989) 2309–2326.
[2] Y. Hori, H. Wakebe, T. Tsukamoto, O. Koga, Electrocatalytic process of CO selectivity in electrochemcial reduction of CO2 at metal electrodes in aqueous media, Electrochim. Acta 39 (1994) 1833–1839.
[3] Y. Hori, A. Murata, Y. Yoshinami, Adsorption of CO, intermediately formed in electrochemical reduction of CO2, at a copper electrode, J. Chem. Soc. Faraday Trans. 87 (1991) 125–128.
[4] H.A. Hansen, J.B. Varley, A.A. Peterson, J.K. Norskov, Understanding trends in the electrocatalytic activity of metals and enzymes for CO2 reduction to CO, J. Phys. Chem. Lett. 4 (2013) 388–392.
[5] K.P. Kuhl, T. Hatsukade, E.R. Cave, D.N. Abram, J. Kibsgaard, T.F. Jaramillo, Electrocatalytic conversion of carbon dioxide to methane and methanol on transition metal surfaces, J. Am. Chem. Soc. 136 (2014) 14107–14113.
[6] D. Kim, C.L. Xie, N. Becknell, Y. Yu, M. Karamad, K. Chan, E.J. Crumlin, J.K. Norskov, P.D. Yang, Electrochemical activation of CO2 through atomic ordering transformations of AuCu nanoparticles, J. Am. Chem. Soc. 139 (2017) 8329–8336.
[7] E.R. Cave, J.H. Montoya, K.P. Kuhl, D.N. Abram, T. Hatsukade, C. Shi, C. Hahn, J.K. Norskov, T.F. Jaramillo, Electrochemical CO2 reduction on Au surfaces: mechanistic aspects regarding the formation of major and minor products, Phys. Chem. Chem. Phys. 19 (2017) 15856–15863.

[8] Z.W. Ulissi, M.T. Tang, J.P. Xiao, X.Y. Liu, D.A. Torelli, M. Karamad, K. Cummins, C. Hahn, N.S. Lewis, T.F. Jaramillo, K.R. Chan, J.K. Norskov, Machine-learning methods enable exhaustive searches for active bimetallic facets and reveal active site motifs for CO2 reduction, ACS Catal. 7 (2017) 6600–6608.
[9] A.A. Peterson, J.K. Norskov, Activity descriptors for CO2 electroreduction to methane on transition-metal catalysts, J. Phys. Chem. Lett. 3 (2012) 251–258.
[10] S. Back, H. Kim, Y. Jung, Selective heterogeneous CO2 electroreduction to methanol, ACS Catal. 5 (2015) 965–971.
[11] S. Sen, D. Liu, G.T.R. Palmore, Electrochemical reduction of CO2 at copper nanofoams, ACS Catal. 4 (2014) 3091–3095.
[12] J.F. Xie, Y.X. Huang, W.W. Li, X.N. Song, L. Xiong, H.Q. Yu, Efficient electrochemical CO2 reduction on a unique chrysanthemum-like Cu nanoflower electrode and direct observation of carbon deposite, Electrochim. Acta 139 (2014) 137–144.
[13] N. Gupta, M. Gattrell, B. MacDougall, Calculation for the cathode surface concentrations in the electrochemical reduction of CO2 in KHCO3 solutions, J. Appl. Electrochem. 36 (2006) 161–172.
[14] C.W. Li, M.W. Kanan, CO2 reduction at Low overpotential on Cu electrodes resulting from the reduction of Thick Cu2O films, J. Am. Chem. Soc. 134 (2012) 7231–7234.
[15] A. Verdaguer-Casadevall, C.W. Li, T.P. Johansson, S.B. Scott, J.T. McKeown, M. Kumar, I.E.L. Stephens, M.W. Kanan, I. Chorkendorff, Probing the active surface sites for CO reduction on oxide-derived copper electrocatalysts, J. Am. Chem. Soc. 137 (2015) 9808–9811.
[16] A. Eilert, F. Cavalca, F.S. Roberts, J. Osterwalder, C. Liu, M. Favaro, E.J. Crumlin, H. Ogasawara, D. Friebel, L.G.M. Pettersson, A. Nilsson, Subsurface oxygen in oxide-derived copper electrocatalysts for carbon dioxide reduction, J. Phys. Chem. Lett. 8 (2017) 285–290.
[17] M. Favaro, H. Xiao, T. Cheng, W.A. Goddard, J. Yano, E.J. Crumlin, Subsurface oxide plays a critical role in CO2 activation by Cu(111) surfaces to form chemisorbed CO2, the first step in reduction of CO2, Proc. Natl. Acad. Sci. U. S. A. 114 (2017) 6706–6711.
[18] F.S. Roberts, K.P. Kuhl, A. Nilsson, High selectivity for ethylene from carbon dioxide reduction over copper nanocube electrocatalysts, Angew. Chem.—Int. Ed. 54 (2015) 5179–5182.
[19] C.W. Li, J. Ciston, M.W. Kanan, Electroreduction of carbon monoxide to liquid fuel on oxide-derived nanocrystalline copper, Nature 508 (2014) 504.
[20] J. Klankermayer, S. Wesselbaum, K. Beydoun, W. Leitner, Selective catalytic synthesis using the combination of carbon dioxide and hydrogen: catalytic chess at the interface of energy and chemistry, Angew. Chem.—Int. Ed. 55 (2016) 7296–7343.
[21] C.W. Machan, M.D. Sampson, C.P. Kubiak, A molecular ruthenium electrocatalyst for the reduction of carbon dioxide to CO and formate, J. Am. Chem. Soc. 137 (2015) 8564–8571.
[22] J.M. Saveant, Molecular catalysis of electrochemical reactions. Mechanistic aspects, Chem. Rev. 108 (2008) 2348–2378.
[23] K.W. Frese, S. Leach, Electrochemical reduction of carbon dioxide to methane, methanol and CO on Ru electrodes, J. Electrochem. Soc. 132 (1985) 259–260.
[24] J.P. Popic, M.L. AvramovIvic, N.B. Vukovic, Reduction of carbon dioxide on ruthenium oxide and modified ruthenium oxide electrodes in 0.5 M NaHCO3, J. Electroanal. Chem. 421 (1997) 105–110.
[25] D. Sebastian, A. Palella, V. Baglio, L. Spadaro, S. Siracusano, P. Negro, F. Niccoli, A.S. Arico, CO2 reduction to alcohols in a polymer electrolyte membrane co-electrolysis cell operating at low potentials, Electrochim. Acta 241 (2017) 28–40.
[26] J.T. Billy, A.C. Co, Experimental parameters influencing hydrocarbon selectivity during the electrochemical conversion of CO2, ACS Catal. (2017) 8467–8479.
[27] I. Platzman, R. Brener, H. Haick, R. Tannenbaum, Oxidation of polycrystalline copper thin films at ambient conditions, J. Phys. Chem. C 112 (2008) 1101–1108.
[28] D.J. Morgan, Resolving ruthenium: XPS studies of common ruthenium materials, Surf. Interface Anal. 47 (2015) 1072–1079.
[29] W. Tang, A.A. Peterson, A.S. Varela, Z.P. Jovanov, L. Bech, W.J. Durand, S. Dahl, J.K. Norskov, I. Chorkendorff, The importance of surface morphology in controlling the selectivity of polycrystalline copper for CO2 electroreduction, Phys. Chem. Chem. Phys. 14 (2012) 76–81.
[30] D. Kim, J. Resasco, Y. Yu, A.M. Asiri, P.D. Yang, Synergistic geometric and electronic effects for electrochemical reduction of carbon dioxide using gold-copper bimetallic nanoparticles, Nat. Commun. 5 (2014) 8.
[31] R. Reske, H. Mistry, F. Behafarid, B.R. Cuenya, P. Strasser, Particle size effects in the catalytic electroreduction of CO2 on Cu nanoparticles, J. Am. Chem. Soc. 136 (2014) 6978–6986.
[32] R. Kas, K.K. Hummadi, R. Kortlever, P. de Wit, A. Milbrat, M.W.J. Luiten-Olieman, N.E. Benes, M.T.M. Koper, G. Mul, Three-dimensional porous hollow fibre copper electrodes for efficient and high-rate electrochemical carbon dioxide reduction, Nat. Commun. 7 (2016) 7.
[33] H. Zhong, K. Fujii, Y. Nakano, Effect of KHCO3 concentration on electrochemical reduction of CO2 on copper electrode, J. Electrochem. Soc. 164 (2017) F923–F927.